



A near-infrared turn-on fluorescence probe for glutathione detection based on nanocomposites of semiconducting polymer dots and MnO₂ nanosheets

Cheng Zheng¹ · Lei Ding^{2,3} · Yanni Wu^{2,3} · Xionghong Tan³ · Yongyi Zeng^{2,3,4} · Xiaolong Zhang^{2,3} · Xiaolong Liu^{2,3} · Jingfeng Liu^{2,3,4}

Received: 1 June 2020 / Revised: 17 August 2020 / Accepted: 11 September 2020

© Springer-Verlag GmbH Germany, part of Springer Nature 2020

Abstract

Fluorescence biosensors that enable highly sensitive detection of glutathione (GSH) are in great demand for various biological investigations and early disease diagnoses. Here, we report a turn-on fluorescence nanoplatform based on fluorescent semiconducting polymer nanoparticle@MnO₂ nanosheets (P-dot@MnO₂) nanocomposites for rapid homogeneous determination of GSH. The near-infrared (NIR) fluorescent P-dots were prepared by doping NIR dyes into polymer matrix and then encompassed by MnO₂, which resulted in a remarkable fluorescence quenching. Owing to the selective decomposition of MnO₂ by GSH, the fluorescence recovery was achieved in the presence of GSH. On the basis of the target-induced turn-on fluorescence response, the developed nanoplatform can readily detect GSH with a high sensitivity up to 0.26 μM, as well as a superior specificity. Furthermore, it was successfully applied in monitoring the intracellular GSH in living cells, revealing its great potential in biomedical applications.

Keywords Manganese dioxide nanosheets · Fluorescent polymer dots · Fluorescence resonance energy transfer · Nanoplatform

Introduction

As the most abundant intracellular nonprotein thiol in mammalian and eukaryotic cells, glutathione (GSH) serves as an essential endogenous antioxidant in numerous crucial

biological systems [1, 2]. The disordering of the GSH level is generally considered to be associated with various human diseases, including liver damage, diabetes, Parkinson's disease, Alzheimer's disease, psoriasis, human immunodeficiency virus (HIV), and cancer, and to some extent reflects the health level [3, 4]. In view of its clinical and biological importance, development of reliable strategies enabling highly sensitive detection of GSH as well as monitoring of intracellular GSH in living cells is favorable for various biological investigations and early disease diagnoses.

Among available analytical technologies, fluorescence spectroscopy has been extensively demonstrated as an important detection and imaging approach for the assay of GSH or evaluating intracellular GSH changes because of the merits of high temporal and spatial resolution, nondestructive properties, rapid response, and real-time monitoring [5–8]. In recent years, 2D layered manganese dioxide nanosheets (MnO₂ NSs) have been discovered to possess superior light absorption capability and strong oxidation ability, which thereby can be developed as a fluorescence quencher and recognition unit for the establishment of fluorescent GSH sensing systems [9, 10]. These constructed biosensors often provide a low

background signal due to the strong fluorescence quenching effect of MnO_2 NSs and produce a turn-on fluorescence response that may result in minimizing the occurrence of false positive signals. Up to now, a series of fluorescent probes have been integrated with MnO_2 NSs to form MnO_2 NS-based nanocomposites for GSH detection, such as organic fluorophores [11], up-converting nanoparticles [12], carbon dots [13], g-C₃N₄ [14], quantum dots (QDs) [15], and polymer fluorescence nanoparticles [16]. However, most employed fluorescent probes emit blue-colored or green-colored fluorescence at the wavelength range of 400–600 nm, which may suffer from relatively weak light penetration into tissue, light scattering in turbid media, and interference of auto-fluorescence from cells or biological samples in the detection and imaging process [17]. Therefore, there is still an urgent need to explore new fluorescence nanoprobe with emission in the red or even near-infrared (NIR) region with long emission wavelength to improve the analytical and imaging performance for GSH sensing.

Currently, semiconducting polymer nanoparticles (P-dots), composed of organic semiconducting π -conjugated polymers, as a new class of promising fluorescent nanomaterials have attracted significant interest that exhibit good chemical stability, tunable surface properties, minimal cytotoxic characteristics, and less emitter-leaching behavior [18, 19]. Inspiringly, most of the recently developed P-dots are capable of generating tunable fluorescence extending from 400 to 750 nm through varying semiconducting polymer components or doping fluorescent emitting unit into matrix of P-dots [20, 21]. Moreover, the fluorescence brightness of P-dots is extraordinarily high, which is reported to be orders of magnitude higher than that of small-molecule dyes, and tens of times better than that of QDs [22]. Due to these impressive photophysical properties, P-dots-based platforms are highly preferable for various biomedical applications for chem/biosensing [23, 24], bioimaging [25], phototherapy [26, 27], and biological photoactivation [28].

In our previous work, we have successfully designed a fluorescence nanoprobe based on P-dots and dopamine-melanin nanosystems for rapid and selective sensing of GSH [29]. Unfortunately, it disables to be used for visualizing the intracellular GSH distribution. Herein, we integrated NIR P-dots with MnO_2 NSs and described a novel nanocomposite-based strategy for detection and imaging of GSH in living cells. The schematic illustration of the established nanoplatform is shown in Fig. 1. A NIR-emitting dye, tetraphenylporphyrin (TPP), was first embedded by poly[(9,9'-dioctyl-2,7-divinylene-fluorenylene)-alt-2-methoxy-5-(2-ethyl-hexyloxy)-1,4-phenylene] (PEPV) chains to form compact spherical P-dots using the nanoprecipitation method. And then, MnO_2 NSs as efficient energy acceptors were grown in situ on the surface of NIR-emissive P-dots to obtain functionalized P-dot@ MnO_2 nanocomposites, which

leads to fluorescence quenching through a Förster resonance energy transfer (FRET) process, whereas P-dot@ MnO_2 nanocomposites were converted back to the initial P-dots accompanied with the fluorescence recovery in the presence of GSH, since GSH can reduce MnO_2 to manganese ions (Mn^{2+}) resulting in the decomposition of MnO_2 . The change of fluorescence signal in form of turn-on constitutes the basis for the GSH sensing. Based on the same principle, the P-dot@ MnO_2 nanocomposites could be applied for monitoring changes of the GSH concentration in living cells. Benefiting from the NIR dye encapsulation and MnO_2 NS coating in the P-dot@ MnO_2 nanocomposites, the proposed nanoplateform is able to offer enhanced NIR fluorescence brightness and prohibit the potential leakage of embedded NIR dye, which make it an improvement of detection reliability and sensitivity.

Experimental

Chemicals and apparatus

The details of chemicals and apparatus used here can be found on Electronic Supplementary Material (ESM).

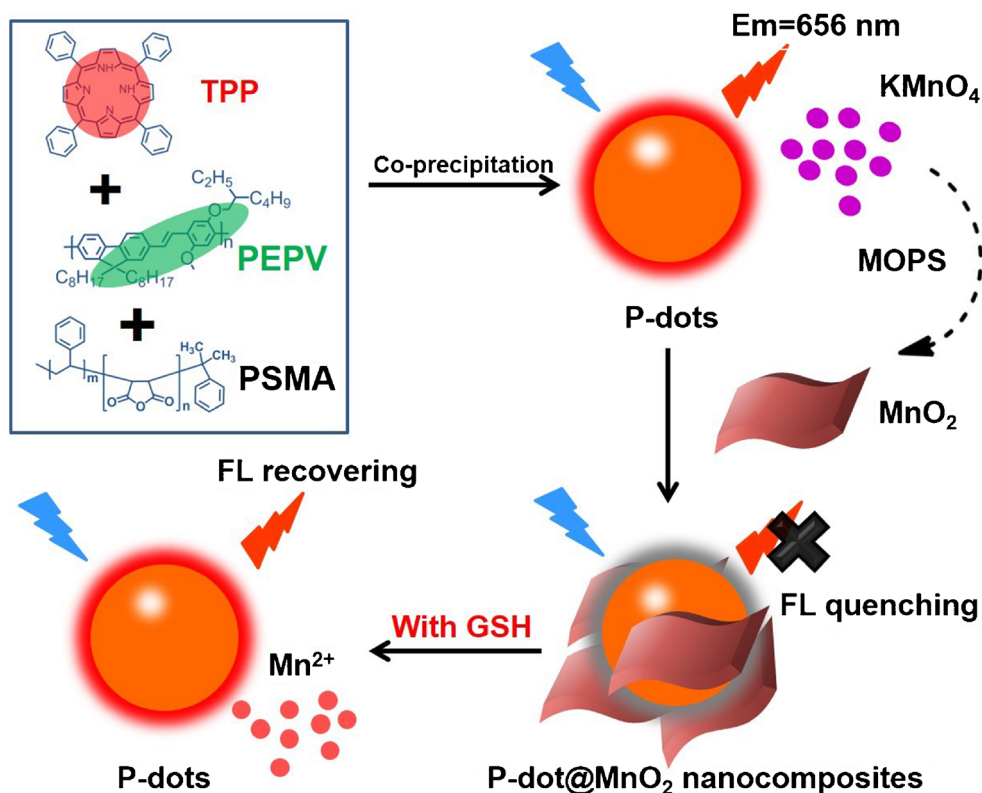
Preparation of P-dots

P-dots were synthesized according to the reprecipitation method of our previously reported work [29, 30]. Briefly, first, PEPV (1 mg), poly(styrene-co-maleic anhydride) (PSMA) (10 mg), and fluorescent dye TPP (0.1 mg) were dissolved together in 1 mL of THF solution with ultrasonic treatment for 2 min to form a homogeneous solution. Subsequently, 1 mL of the mixture solution was added quickly into 10 mL of ultrapure water in a bath sonicator for 5 min. THF was then removed by rotary evaporation at 50 °C and filtered using a 0.2-μm syringe filter to remove possible big aggregates. Thereafter, the reactant was washed three times and concentrated by ultrafiltration. Ultimately, the resultant P-dots solution (about 500 $\mu\text{g mL}^{-1}$) with good dispersibility was obtained by sonicating for a few minutes and stored in the dark at 4 °C before using.

Preparation of P-dot@ MnO_2 nanocomposites

The P-dot@ MnO_2 nanocomposites were prepared by mixing 1 mL of P-dots (500 $\mu\text{g mL}^{-1}$) with 10 mL of KMnO₄ (1 mM) in MOPS (100 mM, pH 7.0) solution. The mixture was sonicated for 30 min until a brown solution formed. Then, the brown mixture was collected by centrifugation at 10,000 rpm for 10 min and washed three times with ultrapure water. Finally, the P-dot@ MnO_2 nanocomposites were redispersed in 10 mL of ultrapure water and stored in the dark at 4 °C before using.

Fig. 1 Schematic representation of the fabrication of the P-dot@MnO₂ nanocomposite-based sensing platform for GSH detection



GSH detection based on P-dot@MnO₂ nanocomposites

For GSH detection, 150 μL of different concentrations of GSH was added into 50 μL of P-dot@MnO₂ nanocomposites solution and then the mixture solution was incubated for 5 min at room temperature. Thereafter, the fluorescence spectra were measured with excitation wavelength at 458 nm. All fluorescence measurements were performed in PBS buffer. The emission intensity at 656 nm was taken for quantitative analysis. In order to make the fluorescence signal within the effective range of the fluorescence spectrophotometer (0–1000 a.u.), 50 μL of the composites was used for the test.

The selectivity of P-dot@MnO₂ nanocomposites was tested by the same process with various interferences, including some metal ions (1 mM of K⁺, Mn²⁺, and Mg²⁺), amino acids (100 μM of L-Glu and L-Gly), proteins (0.05 mg mL^{-1} of HRP, 1 mg mL^{-1} of BSA and HSA), and reducing bioagents (1 mg mL^{-1} of glucose, 50 μM of AA, VE, NADH, and Cys).

Cell culture, cytotoxicity assay, and imaging

HeLa cells (American Type Culture Collection, ATCC, Manassas, VA) were cultured in Dulbecco's modified Eagle's medium (DMEM) supplemented with 10% fetal

bovine serum, penicillin (100 U mL^{-1}), and streptomycin (100 $\mu\text{g} \text{mL}^{-1}$) and incubated at 37 °C with 5% CO₂ humidified air atmosphere. The cytotoxicity of P-dot@MnO₂ nanocomposites and P-dots was tested by CCK-8 assay according to the manufacturer's instructions. HeLa cells (1×10^4 cells per well in 200- μL media) were seeded in 96-well plates for 12 h, and then various concentrations of nanoparticles were added into culture medium and incubated for 24 h before CCK-8 assay. After removing the medium, 10 μL of CCK-8 solution with 90- μL fresh medium was added into each well and further incubated with cells at 37 °C for 30 min. Then, the absorbance at 450 nm was measured by using a microplate reader. The cell viability was expressed as the ratio of the absorbance of sample-treated cells to that of untreated cells. Each result was the average of five wells.

For imaging experiments, HeLa cells were seeded at about 70–80% confluence for 24 h in 35-mm glass-bottom Petri dishes. Thereafter, culture medium containing nanoparticles (50 $\mu\text{g} \text{mL}^{-1}$) were added and further incubated for 3 h. The cells were washed with cold PBS three times before fluorescence imaging. To reduce the intracellular GSH content, HeLa cells were first incubated with *N*-methylmaleimide (NMM) (a GSH scavenger, 500 μM) for 30 min. The fluorescence images were observed on a confocal laser scanning microscope with an excitation wavelength of 488 nm.

Results and discussion

Synthesis and characterization of P-dots and P-dot@MnO₂ nanocomposites

P-dots with NIR dye-doping are synthesized by using TPP as NIR chromophores, PEPV as the semiconducting polymer matrix, and PSMA as the stabilizing agent via a modified nanoprecipitation method. During nanoparticle preparation, amphiphilic PSMA molecules are hydrolyzed in the aqueous environment to form the main vehicle to encapsulate hydrophobic PEPV and TPP [31]. The joint effect of π - π interaction and hydrophobic force helps the attachment of TPP on P-dots. The carboxyl groups generated from PSMA helped the deposition of MnO₂ on the P-dots. The morphologies of the prepared P-dots and P-dot@MnO₂ nanocomposites were observed with transmission electron microscopy (TEM). Figure 2a shows P-dots had a sphere-like morphology with an average diameter about 80 nm. The in situ preparation of MnO₂ NSs on P-dots surface is accomplished by sonication-induced reduction of KMnO₄ in MOPS solution. As seen in the TEM image of P-dot@MnO₂ nanocomposites in Fig. 2b and Fig. S1 (see ESM), wrinkles and transparency MnO₂ NSs were attached on the P-dots

surface. The HR-TEM presented the polycrystalline structure of MnO₂ NSs (Fig. S2 in ESM), and these two lattice spacing distances of 0.24 and 0.29 nm correspond to {111} and {020} facets of δ -phase MnO₂, respectively. The TEM-EDX also proved the deposition of MnO₂ on the P-dots (Fig. S3 in ESM). Meanwhile, the average size enlarged to 220.2 nm in comparison with the hydrodynamic size of P-dots (122 nm) revealed by the dynamic light scattering (DLS) results from Fig. S4 (see ESM). X-ray photoelectron spectroscopy (XPS) and surface zeta potential analysis were employed to further ascertain presence of MnO₂ NSs in P-dot@MnO₂ nanocomposites. The XPS spectrum of P-dot@MnO₂ nanocomposites presented two peaks located at 642.0 and 653.9 eV, corresponding to Mn 2p of MnO₂ (Fig. 2c). Figure 2d indicates that the zeta potential of P-dots was -26 mV owing to hydrophilic carboxylic acid groups on their surface, while the zeta potential of P-dot@MnO₂ nanocomposites reduced to -48 mV after the MnO₂ NS formation. The Fourier transform infrared (FTIR) spectrum of P-dots showed the characteristic peaks: C–H vibration (2830 cm^{-1}) and C=C stretching (1500 cm^{-1}) of aromatic ring, C=O stretching vibration (1716 cm^{-1}) of the carboxyl group. After coating of MnO₂, the Mn–O vibrations (510 cm^{-1}) appeared (see ESM Fig. S5).

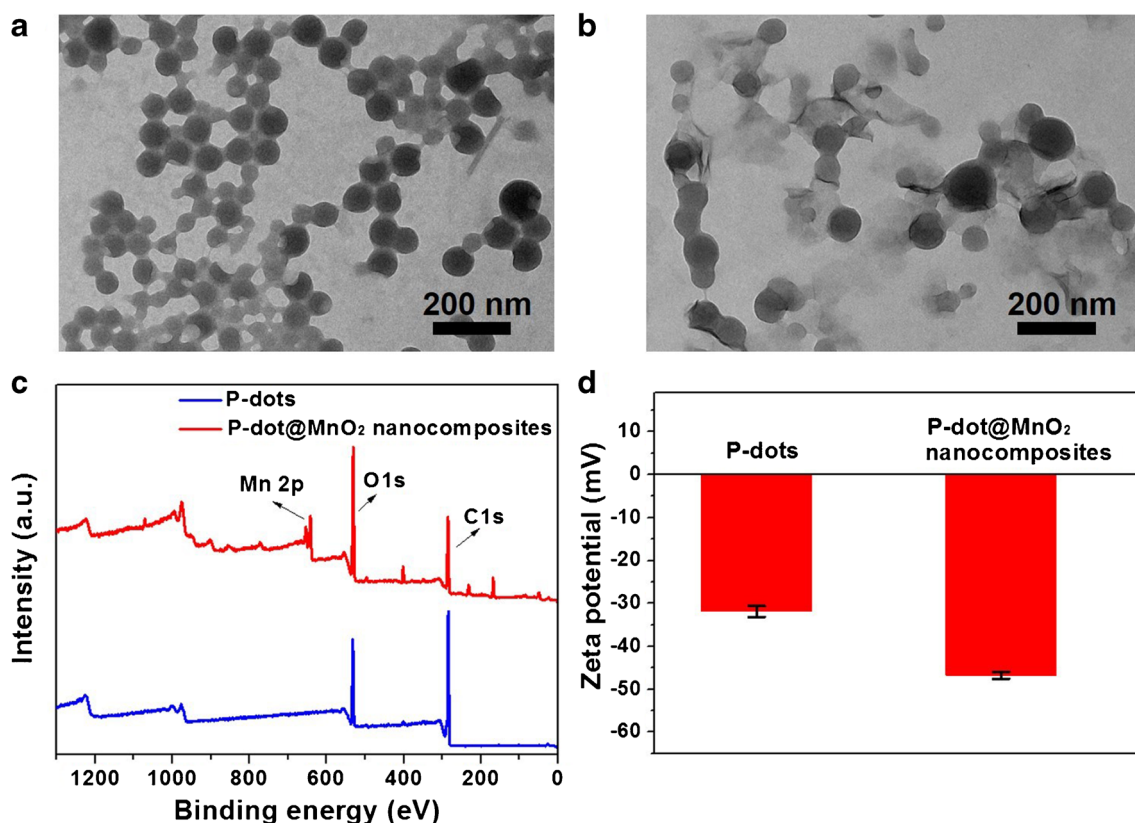


Fig. 2 TEM images of P-dots (a) and P-dot@MnO₂ nanocomposites (b). X-ray photoelectron spectra (c) and surface zeta potential (d) of P-dots and P-dot@MnO₂ nanocomposites

These characterization results support the successful preparation of P-dots and P-dot@MnO₂ nanocomposites.

Optic properties of P-dots, MnO₂ nanosheets, and P-dot@MnO₂ nanocomposites

In our design, PEPV serves as not only the building blocks of P-dots matrix but also the light-harvesting agent that transfers energy to the doped dye TPP. The reason for choosing TPP and PEPV as the energy donor and acceptor pair is that the fluorescence emission spectrum of PEPV overlaps well with the excitation spectrum of TPP, which can trigger an efficient intraparticle energy transfer process (see ESM Fig. S6). To validate the energy transfer between TPP and PEPV, the fluorescence spectra of PEPV, TPP, and P-dots with and without encapsulated TPP were measured. As shown in Fig. S7 (see ESM), PEPV P-dots had only an emission peak at 510 nm attributed to PEPV. Nevertheless, P-dots with TPP doping displayed a strong characteristic fluorescence peak of TPP at 656 nm and 720 nm, and emission from PEPV was relatively weaker, suggesting an efficient conversion of the fluorescence signal from green to NIR regions. To improve the NIR fluorescence brightness of P-dots, we optimized the synthesis condition of P-dots by comparing the fluorescence intensity changes of different P-dots synthesized by varying the doping level of TPP. An obvious luminescence reduction from PEPV was induced by TPP encapsulation. In parallel, as the doping TPP content gradually increased, the NIR fluorescence at 656 nm and 720 nm arising from TPP was enhanced and reached its plateau at 10 wt% (Fig. 3a). Hence 10 wt% was selected as the optimized feeding ratio of PEPV versus TPP. In addition, in the UV-Vis absorption spectrum of P-dots (Fig. 3b), we found that P-dots possessed two characteristic absorption peaks at about 410 nm and 450–500 nm, corresponding to TPP and PEPV, respectively.

Figure 3c described the UV-Vis absorption properties of P-dots, MnO₂ NSs, and P-dot@MnO₂ nanocomposites. It is observed that MnO₂ NSs exhibited broad and monotonic extended absorbance range from the UV to NIR region. As for P-dot@MnO₂ nanocomposites, the characteristic absorption peaks attributed to P-dots were smoothed to form an intense broad band like that of MnO₂ NSs. Furthermore, the fluorescence emission properties of P-dots, MnO₂ NSs, and P-dot@MnO₂ nanocomposites were measured under an excitation source of 458 nm shown in Fig. 3d. There was almost no fluorescence emission detected for the MnO₂ NS solution. When modified with MnO₂ NSs, as expected, the fluorescence intensity of P-dot@MnO₂ nanocomposites at peak of 656 nm was significantly decreased, which may result from the FRET between P-dots and MnO₂ NSs and/or inner filter effects of MnO₂ NSs [32]. Such a strong remarkable quenching effect can provide a low detection background for GSH sensors.

Next, an optimization experiment for the preparation condition of P-dot@MnO₂ nanocomposites was carried out by evaluating the effect of different concentrations of KMnO₄ on their fluorescence intensity. As shown in Fig. 4a, along with increasing the concentration of KMnO₄, the emission peaks at 656 nm and 720 nm simultaneously gradually decreased, revealing more and more MnO₂ grew and deposited on the surface of P-dots. We also found the quenching ability of MnO₂ NSs to P-dots was very high even at a low concentration. It is clearly observed that the quenching efficiency can be up to 90% when KMnO₄ was used at 0.25 mM and finally came to equilibrium over 1 mM (Fig. 4b). Therefore, 1 mM was chosen as the optimum KMnO₄ concentration for the nanocomposite preparation. The ICP-OES result showed that the content of Mn element in P-dot@MnO₂ nanocomposites (1 mg/mL) was about 83 µg/mL. Meanwhile, the fluorescence intensity changes of P-dot@MnO₂ nanocomposites were also seen in Fig. 4c, in which red fluorescence faded away accompanied with the increase of KMnO₄ concentration. For comparison, the solution color of P-dot@MnO₂ nanocomposites became deeper going from light yellow to light brown (Fig. 4d), a similar tendency that can be found in the UV-Vis absorption spectra (see ESM Fig. S8).

P-dot@MnO₂ nanocomposite-based nanoplateform for GSH detection

On the basis of the significant fluorescence quenching ability of MnO₂ NSs as well as selective decomposition of MnO₂ NSs by GSH, a sensing nanoplateform using P-dot@MnO₂ nanocomposites for GSH detection is explored. The feasibility of the constructed nanoplateform was first examined. From the fluorescence spectra given in Fig. 5a, it is obvious to see a notable fluorescence quenching when MnO₂ NSs were coated on the surface of P-dots. Subsequently, distinct fluorescence recovery of nanoplateform appeared with the addition of GSH. This is because MnO₂ NSs are reduced to Mn²⁺ by GSH, and thereby the MnO₂ NS-mediated FRET process is inhibited. The “signal off-on” phenomenon also can be proved by the fluorescence change of the above solution exposure to UV light (inserted pictures of Fig. 5a). We took a further step to evaluate the reaction kinetics of GSH with P-dot@MnO₂ nanocomposites. Figure 5b exhibited a time-dependent evolution of the fluorescence recovery of the nanoplateform caused by GSH. With time elongation, the fluorescence intensity of P-dots sharply increased and only took 4 min to reach the maximum, suggesting a fast redox reaction between GSH and MnO₂. In this regard, the nanoplateform holds considerable promise for design and development of point-of-care testing to realize rapid detection and quantification of GSH.

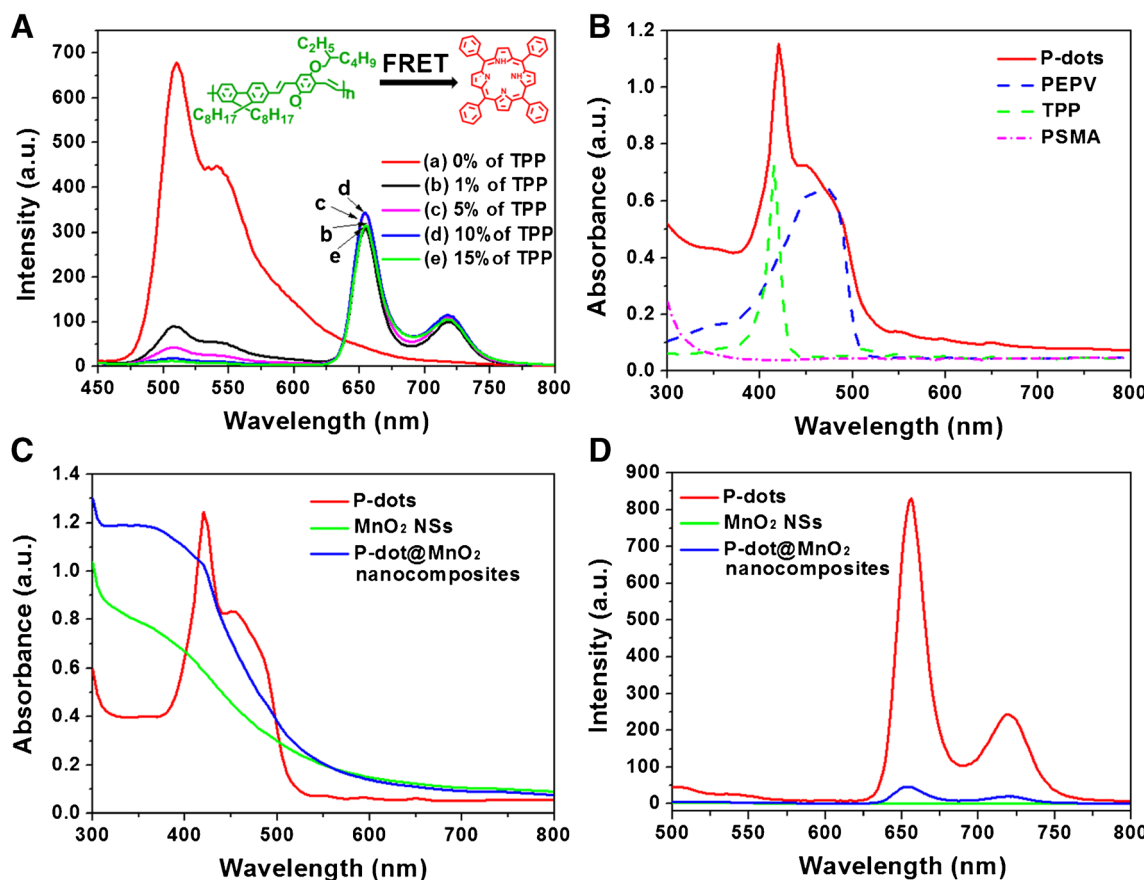


Fig. 3 (A) Fluorescence spectra of P-dots at different doping contents presented as the weight percentage of TPP in the P-dots. The excitation wavelength was 430 nm. (B) UV-Vis absorption spectra of P-dots, free

PEPV, free TPP, and free PSMA. UV-Vis spectra (C) and fluorescence spectra (D) of P-dots, MnO₂ NSs, and P-dot@MnO₂ nanocomposites. The excitation wavelength was 458 nm

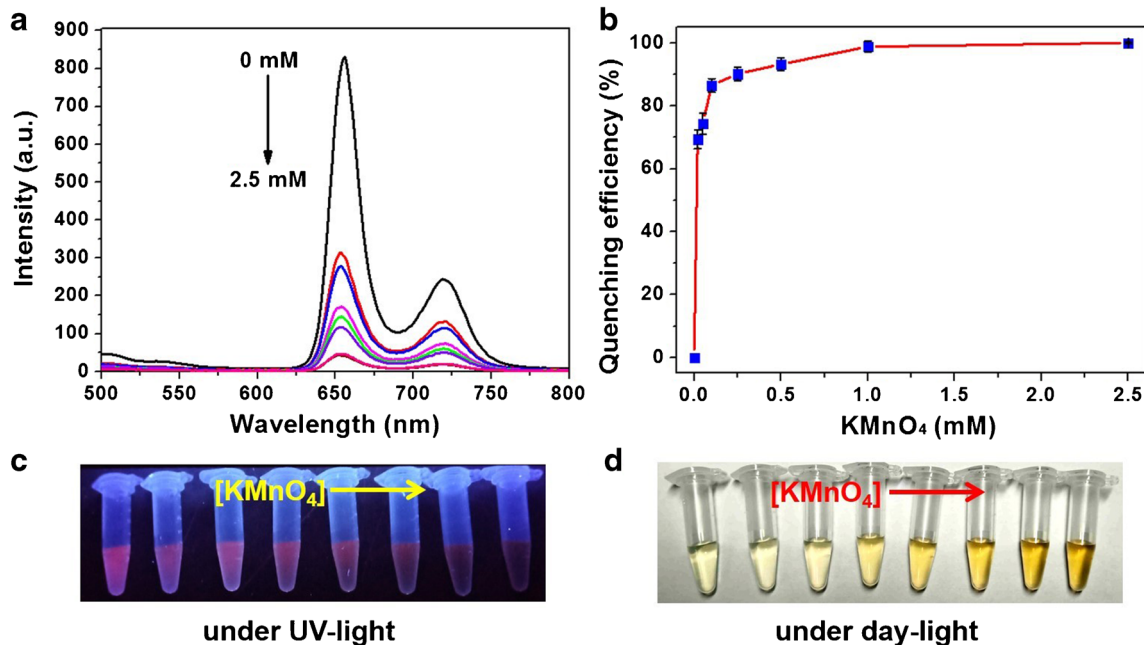


Fig. 4 a Fluorescence spectra of P-dot@MnO₂ nanocomposites synthesized by different concentrations of KMnO₄. b The quenching efficiency of MnO₂ NSs to P-dots as a function of KMnO₄ concentration.

The excitation wavelength was 458 nm. Pictures of P-dot@MnO₂ nanocomposites with various KMnO₄ dosages under UV light (c) and day light (d)

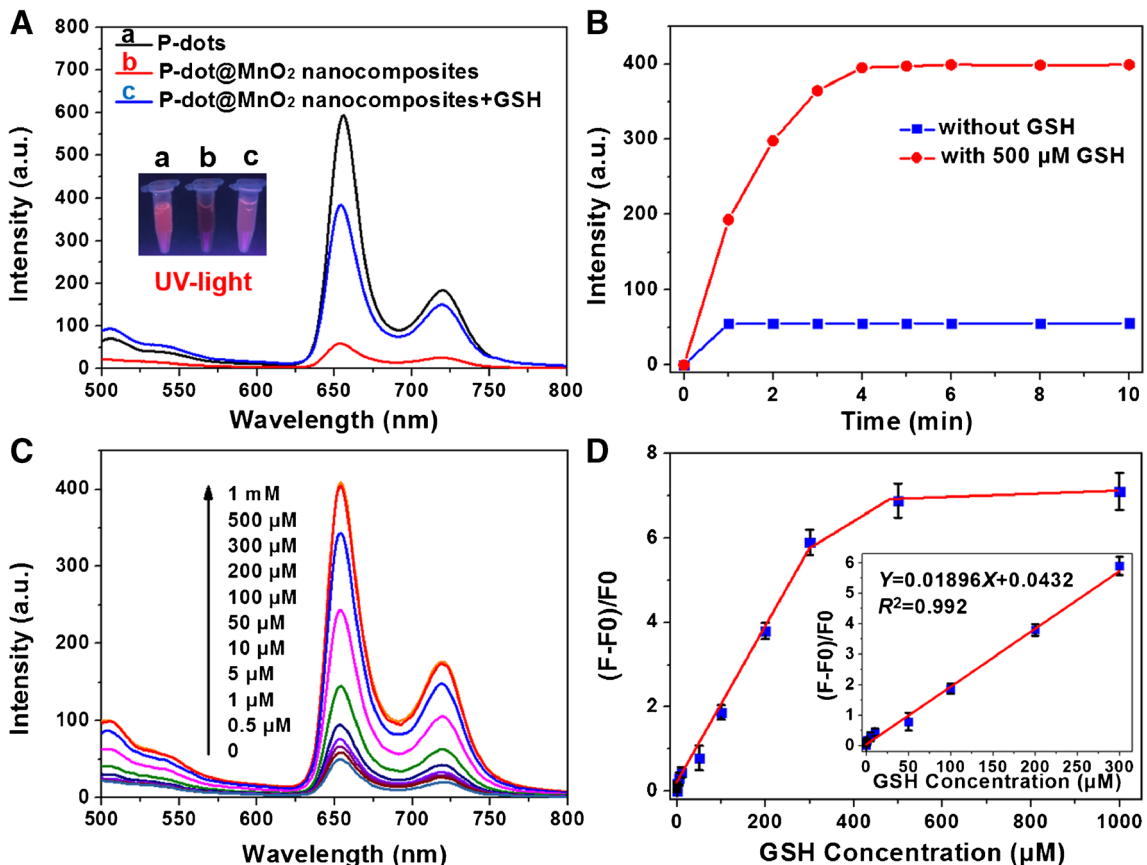


Fig. 5 (A) Fluorescence spectra of (a) P-dots, (b) P-dot@MnO₂ nanocomposites, and (c) P-dot@MnO₂ nanocomposites with 500 μM GSH. Inset: photography showing the corresponding solutions under UV light and day light. (B) Fluorescence intensity of P-dot@MnO₂ nanocomposites at 656 nm with the time after incubation with and without 500 μM GSH. (C) GSH concentration-dependent fluorescence

spectra of P-dot@MnO₂ nanocomposites in the presence of different GSH concentrations. The excitation wavelength was 458 nm. (D) The fluorescence enhancement ratio $((F-F_0)/F_0)$ was plotted as a function of the GSH concentration (0–1 mM). The inset shows the corresponding linear range of the calibration curve for GSH detection. Error bars represent the standard deviation from three independent experiments

We studied the analytical performance of nanoplateform for determination of GSH. As illustrated in Fig. 5c, the fluorescence intensity of the system showed a different degree of increase by adding the concentrations of GSH from 0 to 1 mM. The corresponding calibration curve was constructed using fluorescence enhancement ratio $((F-F_0)/F_0)$ against the concentration of GSH, where F_0 and F were the fluorescence intensity of P-dot@MnO₂ nanocomposites at 656 nm in the absence and presence of GSH, respectively (Fig. 5d). When the GSH concentration was increased over 300 μM, the fluorescence increasing rate of the system becomes slower. As depicted in the inset of Fig. 5d, the fluorescence enhancement ratio was linear to the concentrations of GSH at a range from 0.5 to 300 μM ($R^2 = 0.992$). The interbatch reproducibility study showed a similar result for GSH detection, indicating good interbatch reproducibility (see ESM Fig. S9). The limit of detection (LOD) for this method was low to 0.26 μM based on the definition of three times the deviations of the blank signal (3σ). Moreover, the LOD was compared with that obtained in other previously established approaches for GSH detection. Table S1 (see ESM) makes clear that this sensing

nanoplateform has comparable or even superior sensitivity to the reported strategies [12, 15, 33–37]. The stability of the as-prepared nanocomposites was monitored during 10 days for GSH detection, supporting their good stability (see ESM Fig. S10).

Selectivity of the P-dot@MnO₂ nanocomposite-based nanoplateform

Considering the real applications in bioanalysis and bioimaging, we attempted to test the biological specificity of the proposed nanoplateform. Some potentially competing interferences including metal ions, amino acids, proteins, and reducing bioagents as controls were introduced to investigate fluorescence response of the nanosystem. In Fig. 6, the fluorescence signal of the system exhibited an inconspicuous increase after those interfering agents were added. Conversely, GSH was able to induce a prominent fluorescence enhancement at concentrations from 50 to 500 μM. Note that cysteine (Cys) and ascorbic acid (AA) also can provide the modest fluorescence signal to this nanoplateform (Fig. 6b). However,

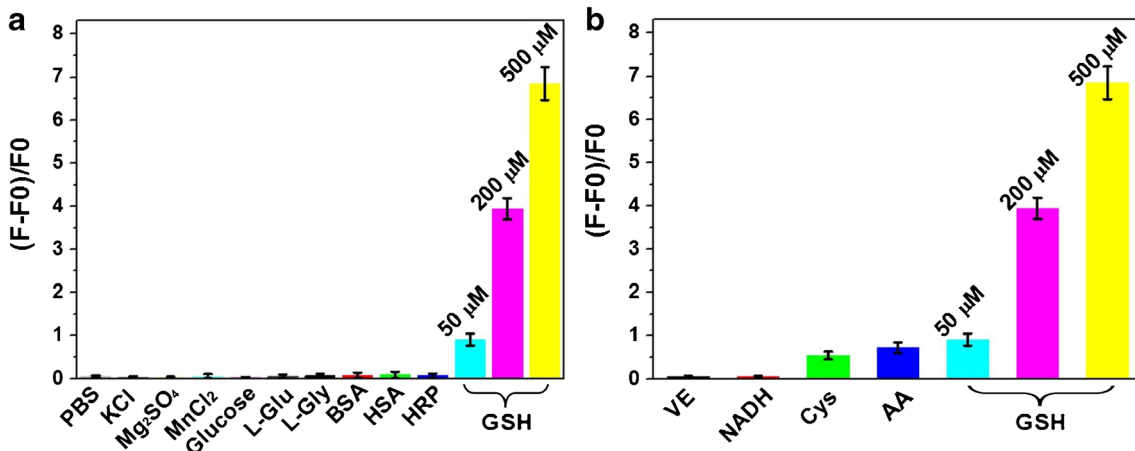


Fig. 6 The fluorescence enhancement ratio ($(F-F_0)/F_0$) of the nanoplatform after incubation with some different analytes including (a) metal ions (1 mM of K^+ , Mg^{2+} , and Mn^{2+}), glucose (1 mg mL⁻¹), amino

the influence of Cys and AA to the selectivity of the nanoplatform could be negligible when the nanoplatform is applied for imaging of intracellular GSH, since the amount of Cys and AA in living cells is at the micromolar level, much smaller than that of GSH in biological systems (at the mM level) [1, 14, 37]. These results indicate that the P-dot@MnO₂ nanocomposite-based nanoplatform is selective for efficient recognition of GSH.

P-dot@MnO₂ nanocomposite-based nanoplatform for monitoring intracellular GSH levels

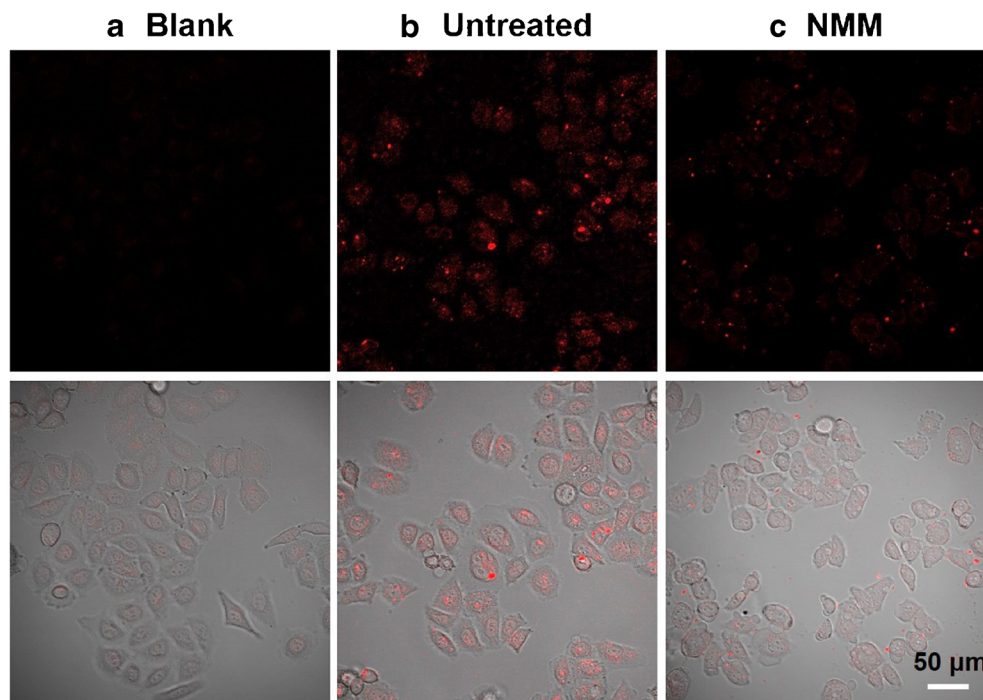
Having confirmed a superior performance for selective analysis of GSH, the P-dot@MnO₂ nanocomposites were further

acids (100 μ M of L-Glu and L-Gly), proteins (1 mg mL⁻¹ of BSA and HAS, and 0.05 mg mL⁻¹ HRP), and GSH; (b) reducing bioagents (50 μ M of VE, NADH, Cys, and AA) and GSH

expanded to assess their potential as fluorescence imaging probes for monitoring cellular GSH. We first evaluated the cytotoxicity of P-dots and P-dot@MnO₂ nanocomposites on HeLa cells, taken as a typical cancer cell. The result of CCK-8 assay is shown in Fig. S11 (see ESM). There was no apparent cell inhibition effect on HeLa cells at all tested concentrations after incubation for 24 h. Both P-dots and P-dot@MnO₂ nanocomposites have good biocompatibility, implying that they could work as appropriate candidates for biomedical applications.

Owing to the millimolar range (0.5–10 mM) of endogenous GSH levels [1], the nanoplatform can be subjected to visualize intracellular GSH in living cells. HeLa cells were incubated with P-dot@MnO₂ nanocomposites; afterwards,

Fig. 7 Fluorescence microscopic images of (a) HeLa cells only, (b) HeLa cells treated with P-dot@MnO₂ nanocomposites, and (c) HeLa cells treated with NMM as well as P-dot@MnO₂ nanocomposites. Top panels: fluorescence microscopy images; bottom panels: the overlap of fluorescence and bright-field images. The concentration of P-dot@MnO₂ nanocomposites was 50 μ g mL⁻¹ and incubated for 3 h. The excitation wavelength was 458 nm



the fluorescence images of HeLa cells were recorded by confocal laser scanning microscopy. No obvious fluorescence signal appeared in blank HeLa cells with no treatment (Fig. 7a). On the contrary, an intense homogeneous red fluorescence can be observed in the cytoplasm of the cell under excitation at 458 nm (Fig. 7b). It indicates that the P-dot@MnO₂ nanocomposites are membrane-permeable and can react with intracellular GSH to provide visible fluorescence signal. To verify our nanoplateform for response to the alterations of intracellular GSH concentrations, HeLa cells were pretreated with the GSH scavenger NMM before incubation with the P-dot@MnO₂ nanocomposites. As depicted in Fig. 7c, there was much lower fluorescence recorded for HeLa cells, revealing that cellular reduction of the MnO₂ NSs is inhibited owing to the decrease of intracellular GSH by NMM. Overall, the cell imaging experiments demonstrate that the proposed nanoplateform is suitable for monitoring the variations of GSH in living cells and would be of great value in a detailed understanding of GSH-related pathophysiological events.

Conclusion

In summary, we have successfully fabricated a novel turn-on fluorescence nanoplateform based on P-dot@MnO₂ nanocomposites to achieve rapid, sensitive, and reliable detection of GSH with a detection limit of 0.26 μM. Endowed by the signal off-on design and the NIR emission properties of P-dots, the as-developed nanoplateform can effectively avoid false positive signals and auto-fluorescence interference from biological samples. Additionally, the strong fluorescence quenching ability of the coated MnO₂ NSs leads to a low background fluorescence and hence an improved signal-to-noise ratio. More importantly, the nanoplateform can be utilized to monitor the GSH level change in live cells considering the good biocompatibility of P-dot@MnO₂ nanocomposites. We envision that this work would provide a convenient and general strategy to design nanocomposite-mediated luminescence assays for GSH sensing and have a good potential in biomedical applications.

Funding This work was supported by the National Natural Science Foundation of China (Grant No. 21605021), the China Postdoctoral Science Foundation (Grant No. 2019M652241), the Young and Middle-Aged Talent Training Project of Fujian Provincial Health and Family Planning Commission (Grant No. 2018-ZQN-75), the Medical Innovation grant of Fujian Province (Grant No. 2018-CX-49), and the Startup Fund of Mengchao Hepatobiliary Hospital of Fujian Medical University (Grant No. QDZJ-2017-004).

Compliance with ethical standards

Conflict of interest The authors declare that they have no competing interests.

References

- Forman HJ, Zhang H, Rinna A. Glutathione: overview of its protective roles, measurement, and biosynthesis. *Mol Asp Med*. 2009;30:1–12.
- Valko M, Rhodes CJ, Moncol J, Izakovic M, Mazur M. Free radicals, metals and antioxidants in oxidative stress-induced cancer. *Chem Biol Interact*. 2006;160:1–40.
- Estrela JM, Ortega A, Obrador E. Glutathione in cancer biology and therapy. *Crit Rev Clin Lab Sci*. 2006;43:143–81.
- Mulay SV, Kim Y, Choi M, Lee DY, Choi J, Lee Y, et al. Enhanced doubly activated dual emission fluorescent probes for selective imaging of glutathione or cysteine in living systems. *Anal Chem*. 2018;90:2648–54.
- Chen X, Zhou Y, Peng X, Yoon J. Fluorescent and colorimetric probes for detection of thiols. *Chem Soc Rev*. 2010;39:2120–35.
- Liu Z, Zhou X, Miao Y, Hu Y, Kwon N, Wu X, et al. A reversible fluorescent probe for real-time quantitative monitoring of cellular glutathione. *Angew Chem Int Ed*. 2017;56:5812–6.
- Dong W, Wang R, Gong X, Dong C. An efficient turn-on fluorescence biosensor for the detection of glutathione based on FRET between N,S dual-doped carbon dots and gold nanoparticles. *Anal Bioanal Chem*. 2019;411:6687–95.
- Liao S, Huang X, Yang H, Chen X. Nitrogen-doped carbon quantum dots as a fluorescent probe to detect copper ions, glutathione, and intracellular pH. *Anal Bioanal Chem*. 2018;410:7701–10.
- Chen J, Meng H, Tian Y, Yang R. Recent advances in functionalized MnO₂ nanosheets for biosensing and biomedicine applications. *Nanoscale Horizons*. 2019;4:321–38.
- Ding B, Zheng P, Ma P, Lin J. Manganese oxide nanomaterials: synthesis, properties, and theranostic applications. *Adv Mater*. 2020;32:1905823.
- Yao C, Wang J, Zheng A, Wu L, Zhang X, Liu X. A fluorescence sensing platform with the MnO₂ nanosheets as an effective oxidant for glutathione detection. *Sensors Actuators B Chem*. 2017;252:30–6.
- Deng R, Xie X, Vendrell M, et al. Intracellular glutathione detection using MnO₂-nanosheet-modified upconversion nanoparticles. *J Am Chem Soc*. 2011;133:20168–71.
- Yan X, Song Y, Zhu C, Song J, Du DSX, Lin Y. Graphene quantum dot-MnO₂ nanosheet based optical sensing platform: a sensitive fluorescence “turn off-on” nanosensor for glutathione detection and intracellular imaging. *ACS Appl Mater Interfaces*. 2016;8:21990–6.
- Zhang X-L, Zheng C, Guo S-S, Li J. Turn-on fluorescence sensor for intracellular imaging of glutathione using g-C₃N₄ nanosheet-MnO₂ sandwich nanocomposite. *Anal Chem*. 2014;86:3426–34.
- Peng C, Xing H, Fan X, Xue Y, Li J, Wang E. Glutathione regulated inner filter effect of MnO₂ nanosheets on boron nitride quantum dots for sensitive assay. *Anal Chem*. 2019;91:5762–7.
- Wang X, Wang D, Guo Y, Yang C, Liu Y, Iqbal A, et al. Fluorescent glutathione probe based on MnO₂-phenol formaldehyde resin nanocomposite. *Biosens Bioelectron*. 2016;77:299–305.
- Tian D, Qian Z, Xia Y, Zhu C. Gold nanocluster-based fluorescent probes for near-infrared and turn-on sensing of glutathione in living cells. *Langmuir*. 2012;28:3945–51.
- Lyu Y, Pu K. Recent advances of activatable molecular probes based on semiconducting polymer nanoparticles in sensing and imaging. *Adv Sci*. 2017;4:1600481.
- Rong G, Corrie SR, Clark HA. In vivo biosensing: progress and perspectives. *ACS Sensors*. 2017;2:327–38.
- Li J, Pu K. Development of organic semiconducting materials for deep-tissue optical imaging, phototherapy and photoactivation. *Chem Soc Rev*. 2019;48:38–71.

21. Wu P-J, Kuo S-Y, Huang Y-C, Chen C-P, Chan Y-H. Polydiacetylene-enclosed near-infrared fluorescent semiconducting polymer dots for bioimaging and sensing. *Anal Chem*. 2014;86:4831–9.
22. Pu K, Shuhendler AJ, Rao J. Semiconducting polymer nanoprobe for in vivo imaging of reactive oxygen and nitrogen species. *Angew Chem Int Ed*. 2013;52:10325–9.
23. Chan Y-H, Wu P-J. Semiconducting polymer nanoparticles as fluorescent probes for biological imaging and sensing. Part Part Syst Charact. 2015;32:11–28.
24. Cheng X, Huang Y, Li D, Yuan C, Li Z-L, Sun L, et al. A sensitive polymer dots fluorescent sensor for determination of α -L-fucosidase activity in human serum. *Sensors Actuators B Chem*. 2019;288:38–43.
25. Yu J, Rong Y, Kuo C-T, Zhou X-H, Chiu DT. Recent advances in the development of highly luminescent semiconducting polymer dots and nanoparticles for biological imaging and medicine. *Anal Chem*. 2017;89:42–56.
26. Lyu Y, Zeng J, Jiang Y, Zhen X, Wang T, Qiu S, et al. Enhancing both biodegradability and efficacy of semiconducting polymer nanoparticles for photoacoustic imaging and photothermal therapy. *ACS Nano*. 2018;12:1801–10.
27. Chang K, Liu Z, Fang X, Chen H, Men X, Yuan Y, et al. Enhanced phototherapy by nanoparticle-enzyme via generation and photolysis of hydrogen peroxide. *Nano Lett*. 2017;17:4323–9.
28. Wang Y, Li S, Liu L, Lv F, Wang S. Conjugated polymer nanoparticles to augment photosynthesis of chloroplasts. *Angew Chem Int Ed*. 2017;56:5308–11.
29. Wang J, Zheng C, Tan X, Zheng A, Zeng Y, Zhang Z, et al. Sensitive fluorometric determination of glutathione using fluorescent polymer dots and the dopamine-melanin nanosystem. *Microchim Acta*. 2019;186:568.
30. Wu M, Wu L, Li J, Zhan D, Lan S, Zhang X, et al. Self-luminescing theranostic nanoreactors with intraparticle relayed energy transfer for tumor microenvironment activated imaging and photodynamic therapy. *Theranostics*. 2019;9:20–33.
31. Sun K, Tang Y, Li Q, Yin S, Qin W, Yu J, et al. In vivo dynamic monitoring of small molecules with implantable polymer-dot transducer. *ACS Nano* 2016; 10: 6769–6781.
32. He J, Jiang X, Ling P, Sun J, Gao F. Ratiometric sensing for alkaline phosphatase based on two independent signals from in situ formed nanohybrids of semiconducting polymer nanoparticles and MnO_2 nanosheets. *ACS Omega*. 2019;4:8282–9.
33. Yuan Y, Zhang J, Wang M, Mei B, Guan Y, Liang G. Detection of glutathione in vitro and in cells by the controlled self-assembly of nanorings. *Anal Chem*. 2013;85:1280–4.
34. Wang Y, Lu J, Tang L, Chang H, Li J. Graphene oxide amplified electrogenerated chemiluminescence of quantum dots and its selective sensing for glutathione from thiol-containing compounds. *Anal Chem*. 2009;81:9710–5.
35. Lin S, Cheng H, Ouyang Q, Wei H. Deciphering the quenching mechanism of 2D MnO_2 nanosheets towards Au nanocluster fluorescence to design effective glutathione biosensors. *Anal Methods*. 2016;8:3935–40.
36. Xu Y, Chen X, Chai R, Xin C, Li H, Yin X-B. A magnetic/fluorometric bimodal sensor based on a carbon dots- MnO_2 platform for glutathione detection. *Nanoscale*. 2016;8:13414–21.
37. Zhu S, Wang S, Xia M, Wang B, Huang Y, Zhang D. Intracellular imaging of glutathione with MnO_2 nanosheet@Ru(bpy)₃²⁺-UiO-66 nanocomposites. *ACS Appl Mater Interfaces*. 2019;11:31693–9.

Publisher's note Springer Nature remains neutral with regard to jurisdictional claims in published maps and institutional affiliations.